

Regular Article

# Neuronal cell loss accompanies the brain tissue response to chronically implanted silicon microelectrode arrays

Roy Biran<sup>a</sup>, David C. Martin<sup>b</sup>, Patrick A. Tresco<sup>a,\*</sup>

<sup>a</sup>The Keck Center for Tissue Engineering, Department of Bioengineering, University of Utah, 20S 2030E Bldg. 570 Rm. 108, Salt Lake City, UT 84112, USA

<sup>b</sup>Macromolecular Science and Engineering Center, Department of Materials Science and Engineering, University of Michigan, Ann Arbor, MI 48109, USA

Received 5 November 2004; revised 31 March 2005; accepted 11 April 2005

Available online 19 July 2005

## Abstract

Implantable silicon microelectrode array technology is a useful technique for obtaining high-density, high-spatial resolution sampling of neuronal activity within the brain and holds promise for a wide range of neuroprosthetic applications. One of the limitations of the current technology is inconsistent performance in long-term applications. Although the brain tissue response is believed to be a major cause of performance degradation, the precise mechanisms that lead to failure of recordings are unknown. We observed persistent ED1 immunoreactivity around implanted silicon microelectrode arrays implanted in adult rat cortex that was accompanied by a significant reduction in nerve fiber density and nerve cell bodies in the tissue immediately surrounding the implanted silicon microelectrode arrays. Persistent ED1 up-regulation and neuronal loss was not observed in microelectrode stab controls indicating that the phenotype did not result from the initial mechanical trauma of electrode implantation, but was associated with the foreign body response. In addition, we found that explanted electrodes were covered with ED1/MAC-1 immunoreactive cells and that the cells released MCP-1 and TNF- $\alpha$  under serum-free conditions *in vitro*. Our findings suggest a potential new mechanism for chronic recording failure that involves neuronal cell loss, which we speculate is caused by chronic inflammation at the microelectrode brain tissue interface.

© 2005 Published by Elsevier Inc.

**Keywords:** Brain tissue; Implantation; Silicon; Neuroinflammation; Neurotoxicity

## Introduction

Microelectrode array technology is an analytical tool for studying high-density neuronal activity, and is currently under development as a control and communication interface for a number of neuroprosthetic applications (Nicolelis and Ribeiro, 2002). The emergence of silicon micro-fabrication has yielded increasingly smaller and higher electrode count devices that are capable of recording from greater volumes of neural tissue with improved spatial discrimination (Branner et al., 2001; Csicsvari et al., 2003; Drake et al., 1988; Kipke et al., 2003). Despite substantial technological advances in design, many of the current

devices are unreliable for chronic recording applications in the CNS (Liu et al., 1999). While it is generally believed that the brain tissue response to chronically implanted silicon microelectrode arrays contributes to recording instability and failure, the underlying mechanisms are unclear.

Studies have demonstrated that reactive tissue surrounds implanted arrays (Agnew et al., 1986; Carter and Houk, 1993; Edell et al., 1992; McCreery et al., 1997; Schmidt et al., 1976, 1993; Schultz and Willey, 1976; Szarowski et al., 2003; Turner et al., 1999) that is similar to that observed following the implantation of other materials in the brain and spinal cord (Aebischer et al., 1988; Campioni et al., 1998; Dymond et al., 1970; Edell et al., 1992; Powell et al., 1990; Stensaas and Stensaas, 1976, 1978; Winn et al., 1989; Yuen and Agnew, 1995). The encapsulation response, which varies both spatially and temporally, involves a variety of

\* Corresponding author. Fax: +1 801 585 5151.

E-mail address: [patrick.tresco@utah.edu](mailto:patrick.tresco@utah.edu) (P.A. Tresco).

cells and their secreted matrix including meningeal cells, fibroblasts, and reactive astrocytes. It is thought that the encapsulation reaction insulates the electrode from nearby neurons (Liu et al., 1999; Schultz and Willey, 1976; Turner et al., 1999), possibly hindering diffusion and increasing electrical impedance (Roitbak and Sykova, 1999) and may increase the distance between the recording surface and nearby neuronal cell bodies (Liu et al., 1999).

Despite being the principle target of chronic recording applications, relatively little is known about the fate of CNS neurons in proximity to chronically implanted silicon microelectrode arrays. While the initial penetrating injury directly damages neurons in the path of the implant; the “kill zone” is considered to be a minor consequence with minimal impact on recording capability of such devices (Henze et al., 2000). It is not known, for instance, if neurons are involved beyond the zone of initial mechanical trauma when the electrode remains in place for extended periods of time.

In the current study, using quantitative methods, we determined the spatial distribution of cell-type-specific markers for macrophages, astrocytes, and neurons at the microelectrode–brain tissue interface at 2 and 4 weeks following microelectrode implantation. In order to discriminate between the events associated with the initial penetrating trauma and those associated with the foreign body response, the reaction was compared to time-matched stab wound controls created using identical microelectrodes and implantation technique. We found in addition to the previously described astroglial encapsulation that the foreign body response to chronic microelectrode implants is associated with a persistent inflammatory response consisting of activated microglia and a loss of neurons and their projections in the brain tissue immediately surrounding the microelectrode. Based on our findings, we propose that a new mechanism for chronic recording failure may involve neuronal loss, which we speculate is caused by inflammatory reactions at the microelectrode–brain tissue interface.

## Materials and methods

### *Microelectrodes*

Single shank 16 count silicon microelectrode arrays were fabricated and supplied by the Center for Neural Communication Technology (CNCT) at the University of Michigan (<http://www.engin.umich.edu/facility/cnct/>). All electrodes had the following dimensions: length, 5 mm; width, 200  $\mu\text{m}$  at the base tapering to 33  $\mu\text{m}$  at the tip; thickness, 15  $\mu\text{m}$  along the shank and 2  $\mu\text{m}$  at the tip. All electrodes were sterilized prior to implantation by exposure to UV light for 30 min.

### *Animal surgery*

All procedures involving animals were conducted using sterile technique in accordance with protocols approved by

the University of Utah Institutional Animal Care and Use Committee. Adult male Fischer 344 rats (225 g–250 g) were anesthetized with a cocktail of ketamine (65 mg/kg), xylazine (7.5 mg/kg), and acepromazine (0.5 mg/kg). Upon reaching full depth of anesthesia, the eyes were covered with ophthalmic ointment and the head was shaved. The scalp was disinfected by treatment with isopropanol followed by butadiene. Animals were transferred to a stereotaxic frame (Stoelting Co., Wood Dale, IL) set under a stereomicroscope. A midline incision extending the length of the skull was made. For all implant types, a 3-mm diameter burr hole was created to three quarter's the depth of the skull with a custom fabricated trephinated drill bit held and lowered under stereotactic control. The center of the hole was positioned at coordinates +0.2 mm forward of bregma and 3 mm lateral to bregma. While drilling, sterile PBS was applied to the bit with a 10-cm<sup>3</sup> syringe through a 21 G needle to cool the drill site and reduce heat transfer to the underlying cortical tissue. The remainder of the burr hole was cut by hand using an identical bit held in a pin vise. The cortical bone plug was removed with fine forceps under stereomagnification. The hole was rinsed liberally with sterile PBS to remove bone drill debris and the dura was carefully opened with a 21 G needle. Microelectrodes were held with a pair of fine forceps and lowered into the brain by hand. The electrode was tethered to the skull by filling the burr hole with silicone elastomer to the level of the skull surface (Kwik-cast, World Precision Instruments, Inc., Sarasota, FL). After the silastic was cured, the microelectrode extending above the silastic was cut with fine surgical scissors leaving the top of the electrode flush with the exterior surface of the silastic and the skull surface. The scalp incision was closed with 5/0 silk sutures. A study comparing tissue reactivity around microelectrodes mounted in the conventional manner with an electrical connector mounted to the skull with bone screws and acrylic showed no differences from this approach (data not shown;  $n = 5$ , at 2 and 4 weeks postimplantation).

As a control, stab wounds were created with the same type of microelectrode. After opening the burr hole and opening the dura, a microelectrode was lowered into the brain to the same depth and in the same manner as described above. The microelectrode was immediately withdrawn, the bone plug replaced, and the scalp closed as described.

### *Euthanasia and tissue processing*

At 2 weeks or 4 weeks after implantation or stab wound, animals were terminally anesthetized with a mixture of ketamine (70 mg/kg) and xylazine (30 mg/kg) and perfused transcardially at a flow rate of 50 mL/min with 250 mL of ice-cold PBS, followed by 250 mL of fresh ice-cold 4% (w/v) paraformaldehyde. The brains were removed and the microelectrodes were carefully retrieved with sharp microdissection forceps and processed for immunostaining, while the brains were postfixed overnight in 4% paraformaldehyde

in PBS. Following postfixation, the brains were equilibrated in 20% sucrose in PBS, sectioned at 30  $\mu\text{m}$  on a freezing microtome, and serially collected in PBS.

### Histology and immunostaining

A list of antibodies used, their source, and dilution is listed in Table 1. All antibodies were diluted in blocking solution consisting of 4% (v/v) normal goat serum, 0.3% (v/v) Triton-X-100, and 0.1% (w/v) sodium azide. Approximately 8 tissue sections at the level of the cerebral cortex were immunostained for each marker per electrode tract spanning approximately 1.8 mm of the cerebral cortex. Sections were treated for 1 h with blocking solution at room temperature. Primary antisera were applied overnight at 4°C. After 3 rinses in PBS (15 min per rinse), appropriately matched secondary antibodies were applied for 1 h at room temperature. Alexa-488 and Alexa-594 labeled secondary antibodies were purchased from Molecular Probes (Eugene, OR). Secondary antibodies were diluted in blocking solution to a concentration of 10  $\mu\text{g}/\text{mL}$ . Sections were counterstained with 10  $\mu\text{M}$  DAPI (Molecular Probes). After washing with PBS, sections were mounted onto microscope slides using Fluoromount-G (Southern Biotech) and covered with a coverglass. Retrieved electrodes were immunostained in the same manner as tissue.

### Imaging and quantification

For quantification of spatial signal intensity, digital images were collected using a Coolsnap color CCD (Roper Scientific; Trenton, NJ) attached to a Nikon E600 microscope using Image Pro 4.5 software (Media Cybernetics; Silver Spring, MD). An 8-bit grayscale image was captured at a sub-saturating exposure time for each specimen. The implant site was centered in the camera field and oriented identically for all specimens. Using the same exposure time, an image corresponding to the same coordinates was captured from the contralateral hemisphere. To quantify the extent of reactivity, a modification of the line profile intensity analysis reported by Kim et al. (2004) was used. With the implant site centered in the image and the broader side of the implant cavities oriented in the horizontal axis, 6 equally-spaced horizontal lines were drawn across the image field such that the middle of each line corresponded to the center of the implant site. A correction factor for each pixel position was applied to adjust for the non-homogenous field

illumination of the light source. The medial and lateral margins of the implant cavity were marked on each line such that the first pixel corresponding to tissue on either side of the cavity was set to distance = 0. In this manner, 12 data points were collected for each pixel of every immunostained tissue section. Pixel positions were then converted to real distances by calibrating to an image of a micrometer. Intensity values for each data point were then adjusted to the background fluorescence intensity by subtracting an average background intensity value generated from a control image of the contralateral hemisphere. In this manner, no change over background is indicated by a value of “0”. The data for each condition were pooled and are reported as the mean.

To quantify the abundance of neuronal bodies, digital images were captured as described above. A calibrated grid was overlaid onto each image and the number of NeuN<sup>+</sup> cell bodies was determined by counting. The grid was set to generate 100  $\times$  100  $\mu\text{m}$  bin area. Hence, neuronal number was measured in discrete 100- $\mu\text{m}$  wide bin areas and reported in five discrete locations from 0 to 500  $\mu\text{m}$  from the microelectrode–brain tissue interface. Corresponding measurements from the medial and lateral side of the interface were averaged, and the number for each bin was then normalized to an average neuronal density of the same coordinates determined in the contralateral hemisphere. For documentation purposes, color images were collected with the Coolsnap camera attached to a Nikon E600 microscope or an Olympus FVX confocal microscope.

### Quantification of cytokine release

Explanted microelectrodes were rinsed in sterile PBS and transferred into a tissue culture dish containing 300  $\mu\text{L}$  of DMEM/F12 (Gibco; Grand Island, NY) supplemented with N2 components (Bottenstein and Sato, 1979) and 25  $\mu\text{g}/\text{mL}$  gentamicin. After 24 h, conditioned medium was collected, centrifuged to remove debris, and stored at  $-80^\circ\text{C}$ . The concentrations of monocyte chemotactic protein-1 (MCP-1) and tumor necrosis factor-alpha (TNF- $\alpha$ ) were determined by a two-antibody “sandwich” enzyme-linked immunosorbent assay (ELISA). A capture antibody against rat MCP-1 (BD Bioscience; San Jose, CA) or rat TNF- $\alpha$  (R&D Systems; Minneapolis, MN) was diluted to 2  $\mu\text{g}/\text{mL}$  in PBS and applied overnight to a 100  $\mu\text{L}/\text{well}$  of a 96 well microtiter plate (Microton; Greiner). Plates were blocked for 1 h at 37°C in 1 $\times$  Tris-buffered saline (TBST) containing 1% (w/v) BSA and 0.05% (v/v) Tween 20. Conditioned

Table 1  
Summary of antibodies

Antibody	Antigen	Cell type(s)	Isotype	Concentration ( $\mu\text{g}/\text{mL}$ )	Vendor
CD68 (ED1)	Lysosomal glycoprotein	Microglia, macrophages	Mouse IgG1	1.0	Serotec
CD11b/c (Mac-1)	CR3 complement receptor	Microglia, macrophages	Mouse IgG2 $\alpha$	2.5	Pharmingen
GFAP	Glial fibrillary acidic protein	Astrocytes	Rabbit IgG	4.0	DAKO
Neurofilament-160	Medium neurofilament polypeptide	Neurons	Mouse IgG1	2.4	Sigma
NeuN	Neuronal nuclei	Neurons	Mouse IgG1	5.0	Chemicon

medium (100  $\mu\text{L}/\text{well}$ ) was applied for 2 h at 37°C. Biotinylated detection antibodies against MCP-1 (2  $\mu\text{g}/\text{mL}$ ; BD Bioscience) or TNF- $\alpha$  (0.2  $\mu\text{g}/\text{mL}$ ; R&D Systems) were diluted in blocking medium and 100  $\mu\text{L}/\text{well}$  was applied for 1 h at 37°C. Neutravidin-HRP (Pierce, Rockford, IL) was diluted in blocking medium to 0.2  $\mu\text{g}/\text{mL}$  and 100  $\mu\text{L}/\text{well}$  was applied for 30 min at 37°C. Fluorogenic substrate (QuantaBlu; Pierce) was prepared according to manufacturer's instructions and applied at 100  $\mu\text{L}/\text{well}$ . Generation of fluorescent product was monitored over time using a plate reader equipped with 340 nm excitation and 400 nm emission filters (Synergy HT; Bio-Tek, Winooski, VT). Serial-diluted recombinant standards were used to generate a standard curve from which sample concentrations were calculated.

#### *Animal numbers and statistics*

Animal cohort sizes of at least  $n = 5$  were used for each condition. To assess differences in reactivity between conditions, comparisons of the mean intensity value at discrete distances were evaluated by a two-tailed Student's  $t$  test. The mean number of NeuN<sup>+</sup> cells at discrete distances was compared by one-way ANOVA using a Tamhane's T2 post hoc test. Significance for all tests was determined at  $P < 0.05$ . A Spearman's ranked coefficient followed by a two-tailed  $t$  test for significance (with  $P < 0.05$ ) was calculated to assess the strength of correlation between reactivity and the degree of neuronal loss.

## **Results**

### *Inflammation and reactive gliosis around indwelling microelectrodes*

The cortical brain tissue reaction to indwelling microelectrodes was characterized by a persistent and localized cellular inflammatory response consisting of macrophages and reactive astrocytes (Fig. 1: right panels B, D, F, H). This pattern of reactivity around indwelling microelectrodes differed from microelectrode stab wound controls, which elicited a subtler response that lessened with time (Fig. 1: left panels: A, C, E, G). At 2 and 4 weeks postimplantation (p.i.), the tissue immediately surrounding the microelectrode contained a multilayered and densely packed region of compact ED1<sup>+</sup> cells (Figs. 1B, D). Consistent with a macrophage phenotype, the ED1<sup>+</sup> cells also labeled for the macrophage antigen, Mac-1 (data not shown). Temporally, the reaction was marked by persistent ED1 immunoreactivity at the implant–brain tissue interface (Figs. 2B, D). Analysis of the cohort by spatial intensity profiling indicated the peak ED1 immunoreactivity was within a 50- $\mu\text{m}$  radius of the microelectrode surface and did not significantly change between 2 and 4 weeks ( $P = 0.088$ ,  $t$  test area under the curve) (Figs. 2B, D).

The ED1<sup>+</sup> layer was surrounded by multiple layers of hypertrophied and intensely GFAP<sup>+</sup> reactive astrocytes (Figs. 1F, H). At both 2 and 4 weeks p.i., elevated GFAP expression extended over a distance greater than 500  $\mu\text{m}$  from the microelectrode interface (Figs. 2B, D). There was minimal overlap between the ED1<sup>+</sup> and the GFAP<sup>+</sup> cells. The two cell types segregated into distinct layers often forming a sharply defined interface. This segregation of reactive layers is demonstrated in the spatial intensity profile of the cohort (Fig. 2), which shows average peak reactivity for the two antigens occupy distinct zones in the tissue immediately surrounding the microelectrode.

Indicators of inflammation and reactive gliosis were also observed surrounding stab wound lesions (Figs. 1A, C, E, G); however, the intensity and extent of each marker were significantly lower compared to the time-matched microelectrode group ( $P < 0.01$ ,  $t$  test area under the curve 0–500  $\mu\text{m}$ ) (Figs. 2A, C). Whereas ED1-reactive cells persisted at the microelectrode–brain tissue interface over time (Figs. 2B, D), immunoreactivity for ED1<sup>+</sup> cells at the site of the microelectrode stab wound lesions significantly declined by 4 weeks ( $P = 1.3 \times 10^{-11}$ ,  $t$  test area under the curve between 0 and 50  $\mu\text{m}$ ) (Fig. 2C). GFAP immunoreactivity also diminished significantly by 4 weeks ( $P = 1.2 \times 10^{-20}$ ,  $t$  test area under curve between 0 and 500  $\mu\text{m}$ ), leaving only a slightly elevated compact zone of enhanced GFAP reactivity at the lesion site (Fig. 1G).

In order to determine whether the elevated reactivity surrounding microelectrodes was due to the silastic used to tether the electrodes, the pattern of reactivity was examined in control animals ( $n = 5$ ) that received a sham surgery consisting of only a burr hole and application of the silastic. No significant ED1 or GFAP elevation was detected in cortical tissue beneath the surgical site in response to this treatment (data not shown).

### *Explanted microelectrodes contain activated macrophages*

Microelectrodes retrieved from fixed brains contained a layer of compact ED1<sup>+</sup>/CD11b<sup>+</sup> (OX-42) cells with small nuclei, resembling the cells observed in tissue sections adjacent to the implantation tract that remained following implant retrieval (Figs. 3A–D). No neurofilament<sup>+</sup> immunostaining was detected and GFAP immunoreactive fibers were rarely observed on the surface of the retrieved electrodes. When identified, GFAP<sup>+</sup> material was often in fragments that resembled astrocytic processes, and was attached to the surface of the ED1<sup>+</sup> cell layer rather than directly contacting the electrode surface.

To further examine the phenotype of cells at the brain–microelectrode interface, the secretion of two key pro-inflammatory cytokines, monocyte chemotactic protein (MCP-1) and tumor necrosis factor-alpha (TNF- $\alpha$ ), was examined. Microelectrodes were explanted from a separate cohort of deeply anesthetized animals after 2 weeks, cultured in defined medium, and the conditioned medium

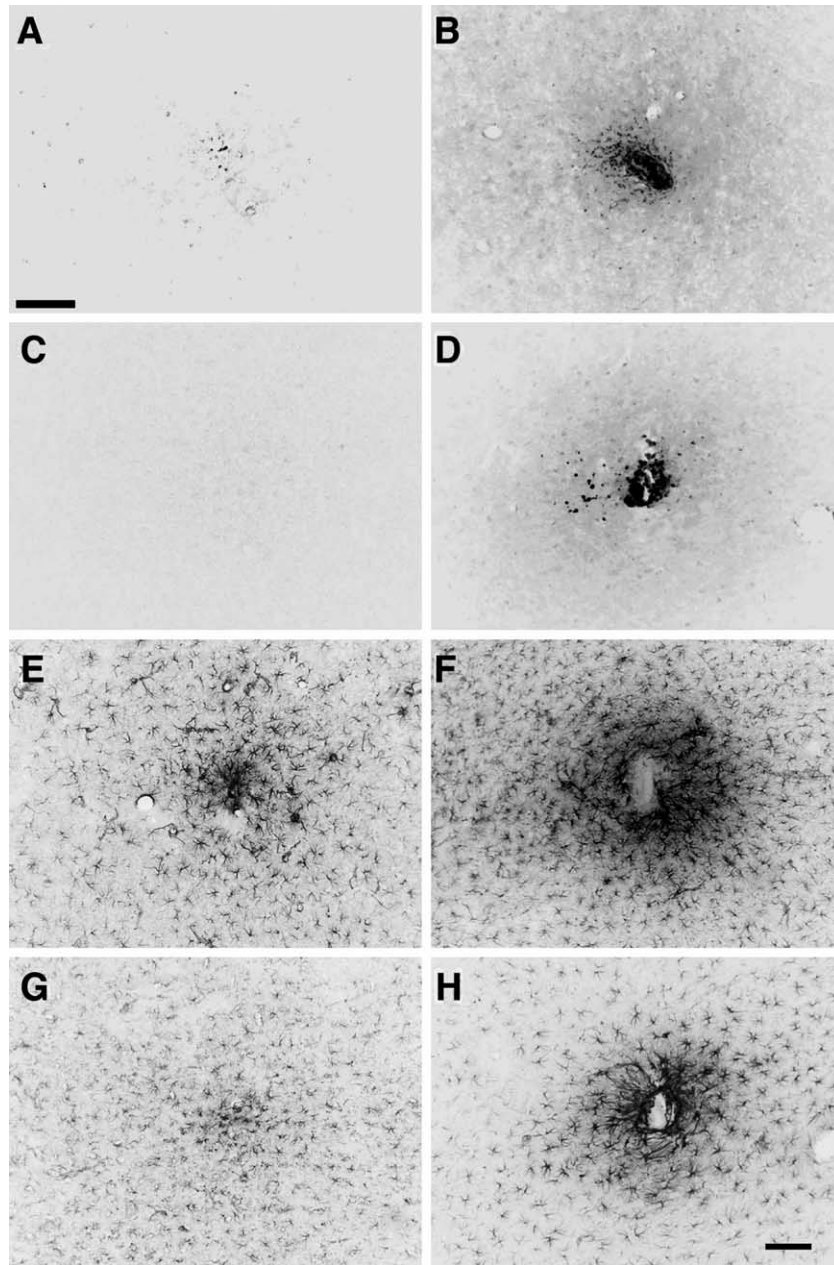


Fig. 1. ED1 and GFAP reactivity to stab wounds (A, C, E, G) and chronically implanted microelectrodes (B, D, F, H) at 2 (A–B, E–F) and 4 weeks p.i. (C–D, G–H), respectively. Representative horizontal inverted fluorescence images demonstrate that ED1 and GFAP reactivity was more intense and extended to a greater distance around implanted microelectrodes (B, D, F, H) compared with time-matched stab wound controls (A, C, E, G). Scale bar = 100  $\mu$ m.

was analyzed by ELISA for cytokines. Like those removed from fixed brains, explanted microelectrodes were also covered with ED1<sup>+</sup>/CD11b<sup>+</sup> cells. Within 1 week of culture, many of the cells migrated away from the electrode and attached to the underlying tissue culture plastic surface (Fig. 3E). The retrieved cells (Fig. 3F) were also identified by live staining and found to react with acetylated low-density lipoprotein (AcLDL) (data not shown), a ligand for macrophage scavenger receptors. The conditioned medium of the explanted macrophages was harvested after the first 24 h in culture and cytokine release was quantified. The medium from single explanted microelectrodes contained detectable

quantities of the pro-inflammatory cytokines MCP-1 and TNF- $\alpha$  (Fig. 3G).

#### *Reduced neuronal density around microelectrodes*

Immunostaining for neurofilament revealed striking reductions in neuronal density surrounding microelectrodes at both 2 and 4 weeks p.i. (Figs. 4B, D). Neurofilament immunostaining at 4 weeks was reduced at the microelectrode–brain tissue interface. Examined as a function of distance from the microelectrode surface, the overall pattern of neurofilament immunoreactivity appeared as the inverse

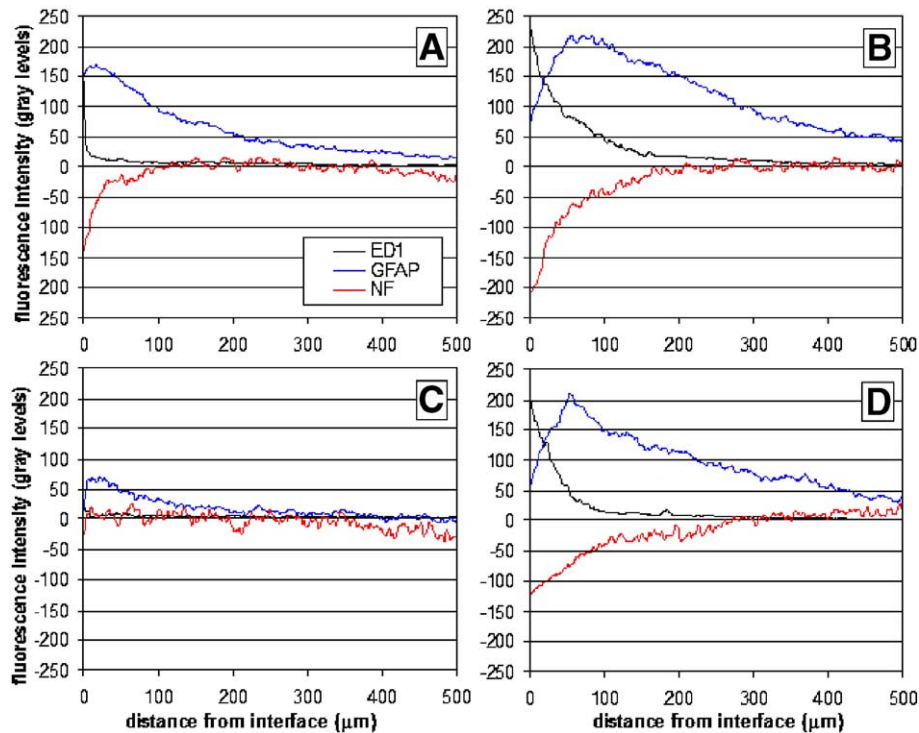


Fig. 2. Quantitative line profile intensity analysis of ED1, GFAP, and neurofilament for all experimental samples. Mean pixel intensity per distance point for 2-week (A–B) and 4-week (C–D) values for stab wounds (A, C) and chronic microelectrodes (B, D) is plotted. The average standard error around each data point ranged from 4% to 14% of the mean value.

of ED1 immunoreactivity (Figs. 2B, D), declining as ED1 intensity increased. There was a strong inverse correlation between ED1 and neurofilament immunoreactivity within 100  $\mu\text{m}$  of the microelectrode interface at both 2 and 4 weeks p.i. (Spearman coefficients of  $-0.976$  ( $P = 1 \times 10^{-6}$ ) and  $-0.995$  ( $P = 1 \times 10^{-6}$ ), respectively). This relationship was not maintained at greater distances from the microelectrode interface suggesting that the stimulus was the foreign body. Lower than normal neurofilament immunoreactivity extended beyond the ED1<sup>+</sup> zone surrounding the microelectrode tracts (Figs. 2B, D). By 4 weeks p.i., the radius of significant neurofilament reduction expanded to a distance of 230  $\mu\text{m}$  from the microelectrode interface (Fig. 2D) ( $P = 0.008$ , area under the curve between 180 and 230  $\mu\text{m}$ ).

Reductions in neurofilament were also observed around stab wounds at 2 weeks (Fig. 4A; Fig. 2A); however, the extent of reduction was smaller compared to that observed around indwelling microelectrodes. Neurofilament loss also exhibited an inverse correlation with ED1 reactivity around stab wounds (Spearman coefficient =  $-0.813$ ,  $P = 1 \times 10^{-6}$ ). In sharp contrast to that observed adjacent to indwelling microelectrodes, neurofilament immunoreactivity around stab wounds was not reduced 4 weeks after surgery (Fig. 4C; Fig. 2C).

To further characterize the impact of the foreign body response on the adjacent neuronal population, the number of NeuN<sup>+</sup> cell bodies was quantified. Here too, we observed a

decline in neuronal cell bodies around the microelectrode implantation tract with an approximate 40% decrease within a 100- $\mu\text{m}$  radius of the microelectrode surface at both 2 and 4 weeks p.i. (Figs. 5B, D, E, F). Beyond 100  $\mu\text{m}$ , there appeared to be only slight reductions in neuronal number, that were not different from adjacent, uninjured areas of the cortex or that observed in the contralateral hemisphere at either time point. In contrast, stab wounds produced no reduction of neurons in the adjacent brain tissue that could be detected by this method at either 2 or 4 weeks (Figs. 6A, C, E, F).

## Discussion

There is a consensus within the recording community that the brain tissue response to chronically implanted silicon microelectrode arrays contributes to recording instability in long-term applications. However, there exists no mechanistic understanding that provides a demonstrable link between electrode-induced histopathology and the erosion of recording capacity. Numerous studies in a variety of experimental models indicate that a general feature of the brain tissue response to chronically implanted electrodes is the presence of an encapsulating layer of reactive astrocytes surrounding the implant interface (Agnew et al., 1986; Carter and Houk, 1993; Edell et al., 1992; McCreery et al., 1997; Schmidt et al., 1976, 1993; Schultz and Willey, 1976; Szarowski et al., 2003; Turner et al., 1999). In addition, the

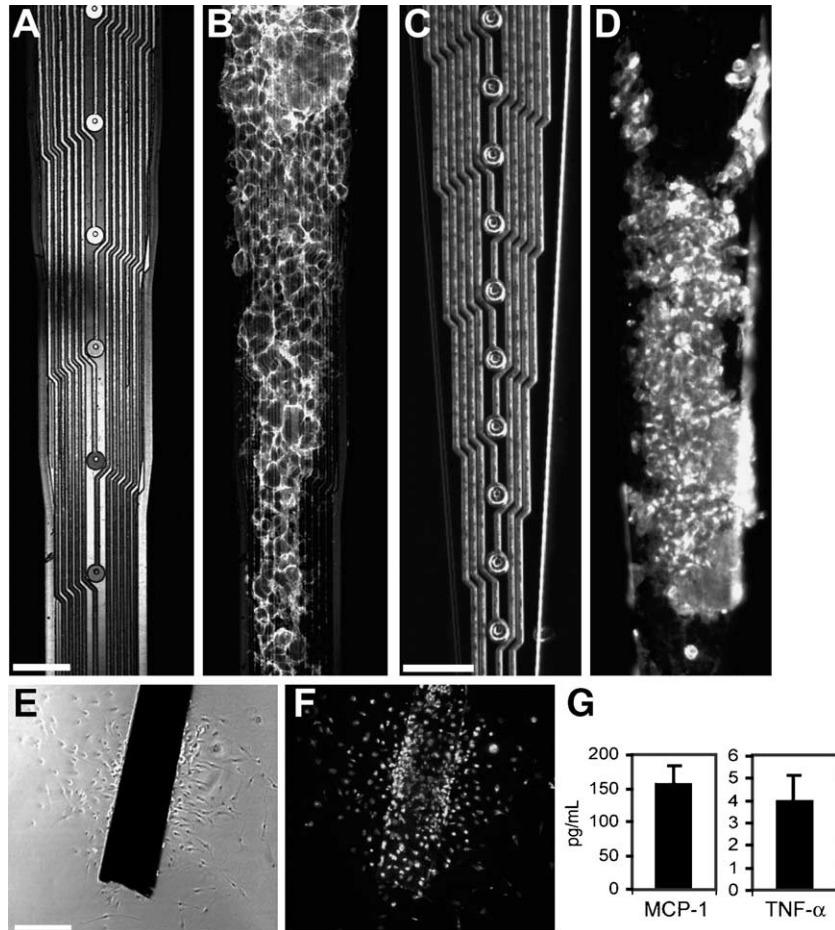


Fig. 3. Retrieved microelectrodes are covered with activated microglia. (A–B) Representative images of the same field showing a microelectrode in brightfield (A) and immunostained for Mac-1 (B) at 2 weeks. (C–D) Brightfield (C) and corresponding ED1 immunostain (D) of a retrieved microelectrode at 2 weeks. Microelectrodes were explanted from living animals and cultured *in vitro* (E–F). By 1 week, macrophages migrated to the culture surface and were identified as ED1<sup>+</sup>. (E) A phase-contrast image of an explanted microelectrode after 1 week in culture shows cells with a migratory morphology on the tissue culture surface. (F) The same field as panel (E) showing ED1-reactivity. (G) Representative data (mean  $\pm$  SEM) of MCP-1 and TNF- $\alpha$  concentrations in conditioned medium harvested from single explanted microelectrodes after the first 24 h following retrieval in serum-free culture. (A–D) Scale bars = 50  $\mu$ m. (E–F) Scale bar = 200  $\mu$ m.

presence of activated microglia in the vicinity of the implanted electrodes has been reported (Turner et al., 1999). This pattern of reactivity has been noted over time points ranging from weeks to months, in rats and cats, suggesting that reactive gliosis is persistent. We observed that the tissue architecture surrounding chronic silicon microelectrode arrays was dramatically different from normal uninjured brain tissue, having a stratified appearance with activated macrophages being the dominant phenotype at the implant–brain tissue interface. Multiple layers of reactive astrocytes resembling a sheath-like encapsulating structure encircled the macrophage rich zone with neurons being largely excluded from each of these zones (Fig. 6).

Current theories hold that the astrocyte ensheathing reaction may be responsible for chronic recording failure by insulating microelectrodes and/or increasing the distance between the electrode and nearby neurons (Edell et al., 1992; Liu et al., 1999; Schultz and Willey, 1976; Turner et al., 1999). The fact that astrocytes swell and divide after

penetrating CNS trauma (Cavanagh, 1970; Mathewson and Berry, 1985) coupled with the finding that the areas of astrogliosis hinder diffusion in the brain (Roitbak and Sykova, 1999) supports a model for astrocyte-mediated erosion of recording capability with this class of devices.

It is also possible that failure of chronic recording directly reflects changes in the viability of the nearby neuronal population. Despite being the target of recording devices, relatively little is known about neurons adjacent to chronic CNS implants. While it is understood that neurons in the path of the microelectrode may be axotomized or killed by direct mechanical trauma during device implantation, the extent of neuronal cell loss has been described as minimal and successful multiunit recording is possible under acute conditions (Henze et al., 2000). However, our observations of the foreign body reaction to chronic indwelling silicon microelectrode arrays raise the possibility that persistent macrophage activation at the microelectrode surface may lead to additional neuronal loss.

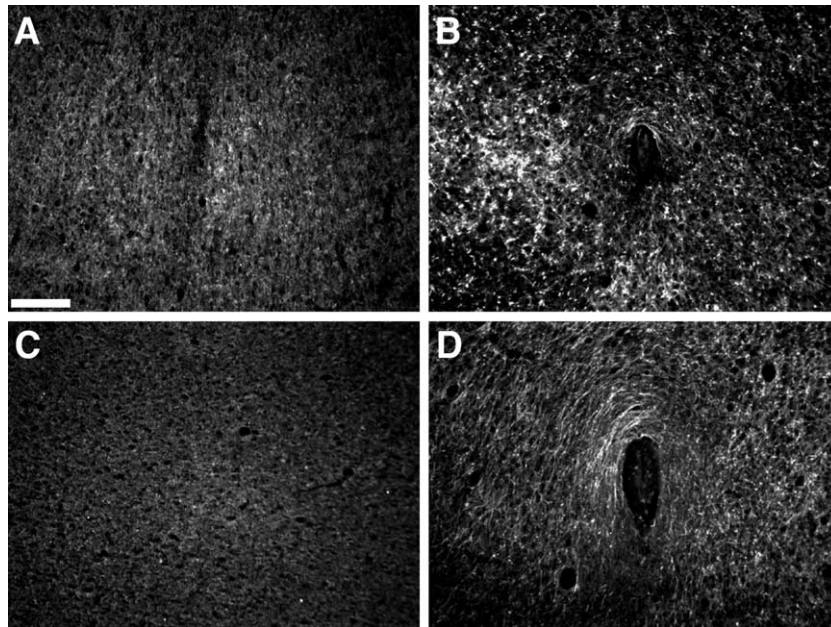


Fig. 4. Neurofilament reactivity to chronically implanted microelectrodes. Representative horizontal fluorescence images of neurofilament immunoreactivity at 2 weeks (A–B) and 4 weeks (C–D) to stab wounds (A, C) and microelectrodes (B, D). Neurofilament reactivity was reduced around microelectrodes (B, D). Stab wounds resulted in comparatively minimal neurofilament loss at 2 weeks (A) and no apparent loss by 4 weeks (C; the lesion site is in the center of the image). Scale bar = 100  $\mu$ m.

Chronic macrophage activation around biomaterial implants in non-nervous tissues is associated with a variety of undesirable outcomes, including implant degradation (Picha et al., 1990; Sutherland et al., 1993), excessive fibrosis (Behling and Spector, 1986), and osteolysis surrounding bone implants (Goldring et al., 1993). While the mechanisms for the recruitment and maintenance of macrophages and microglia around chronic microelectrodes in the CNS are unknown, it is likely that many of the same contributing factors as observed around peripheral implants occur, such as the adsorption of fibrinogen and complement to the device surface (Janatova, 2000; Tang et al., 1996), the subsequent release of pro-inflammatory and cytotoxic cytokines by activated macrophages, and the persistence of activated macrophages around materials that cannot be broken down. Our observation of macrophage activation at the surface of silicon microelectrode arrays and our finding that the cells release of the pro-inflammatory cytokines TNF- $\alpha$  and MCP-1 are consistent with the characteristics of a chronic inflammatory reaction.

The presence of a persistent inflammatory response may have important functional implications for certain types of recording electrodes. Growing evidence suggests that persistently activated microglia found around insoluble plaques in Alzheimer's disease (Luber-Narod and Rogers, 1988) may be a source of local neurotoxicity. In the CNS, like in the periphery, it has been observed that the inability of macrophages to clear insoluble material results in a phenomenon described as "frustrated phagocytosis," which is characterized by increased secretion of inflammatory products that may directly or indirectly cause neuronal

death or alter synaptic activity (Hanisch, 2002). Often, these secreted products also perpetuate microglial activation through autocrine stimulation and by continuing to induce the death of nearby cells.

Microglial-induced neuronal death can be mediated by a myriad of secreted compounds. The most notable microglial-secreted neurotoxic factors include various complement components that can cause neuronal lysis (Gasque et al., 2000; McGeer et al., 1989; Singhrao et al., 2000), cytokines such as TNF- $\alpha$  and IL-1 $\beta$ , which can mediate their effects by direct and indirect pathways (Hanisch, 2002), prostaglandins that indirectly contribute to excitotoxic neuronal death (Rothstein et al., 1993), as well as superoxide anion (Colton et al., 2000) and elevated nitric oxide (Banati et al., 1993; Liu et al., 2002). Even without causing neuronal death, elevated but sublethal doses of TNF- $\alpha$  and other microglial-derived agents can also alter neuronal activity (Hanisch, 2002; Vitkovic et al., 2000), which could contribute to the erosion of single unit activity recording as the inflammatory response around indwelling microelectrodes persists.

Coincident with the persistent inflammatory response, we observed a significant reduction in the abundance of neurons and their projections in the tissue adjacent to the implanted microelectrode arrays. Significant reductions in neurofilament reactivity extended up to 230  $\mu$ m from the microelectrode interface. Similar reductions were observed at 2 weeks, indicating that the majority of neuronal loss occurred early. The loss of neurons could not be accounted for by direct mechanical trauma during implantation of the electrode, as no such loss of neurons occurred around stab

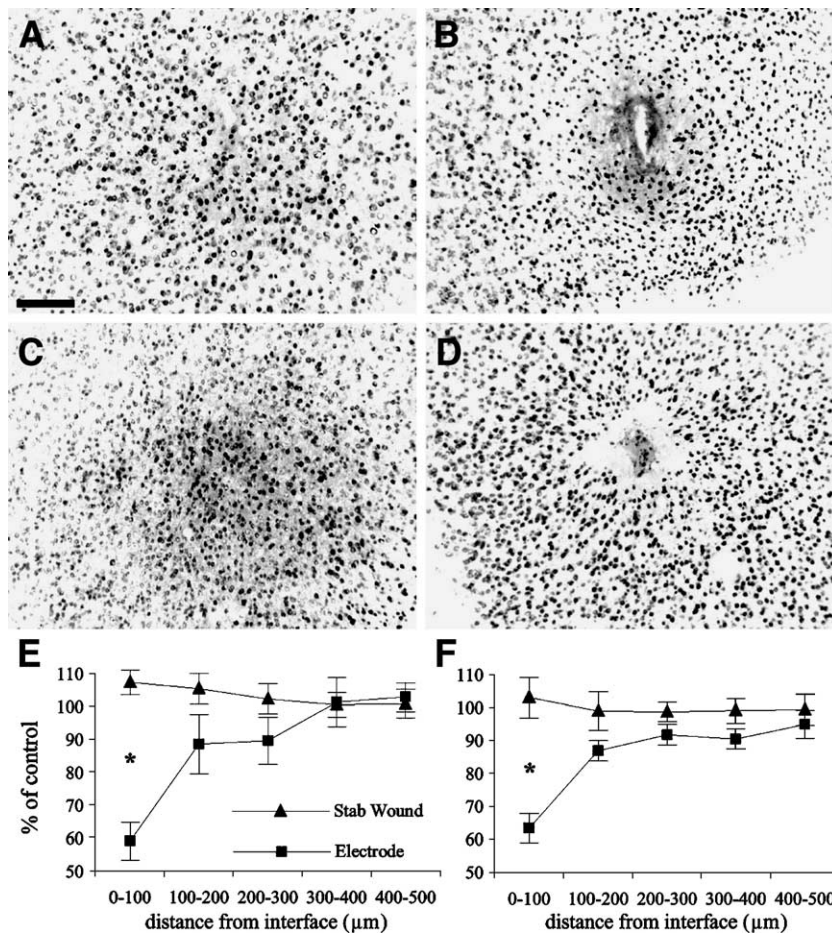


Fig. 5. Neuronal cell body density around chronically implanted microelectrodes. Representative horizontal inverted fluorescence images of NeuN<sup>+</sup> neuronal bodies at 2 weeks (A–B) and 4 weeks (C–D) around stab wounds (A, C) and microelectrodes (B, D). The number of neuronal bodies is reduced in the area adjacent to microelectrodes (B, D) but appears unaltered surrounding stab wound lesions (A, C; lesion site in center of each image). Scale bar = 100 μm. The number of NeuN<sup>+</sup> neurons (mean ± SEM) at 2 weeks (E) and 4 weeks (F) is plotted as a function of 100-μm distance bins from 0 to 500 μm from the microelectrode interface or from the stab wound site. Values were normalized to the average number of NeuN<sup>+</sup> neurons of the uninjured contralateral hemisphere, and are therefore expressed as percent of control. (\*) Indicates a significant difference (ANOVA,  $P < 0.05$ ) between microelectrode and stab wound values for the discrete 100-μm bin in which it appears.

wounds created with identical microelectrodes, and the extent of cell loss was greater than the footprint of the microelectrode itself. Furthermore, the inflammatory reaction to microelectrode stab wounds significantly subsided by 4 weeks suggesting that the stimuli responsible for the early microglial and astrocytic response were no longer present. Hence, the penetrating injury associated with microelectrode implantation does not appear to represent a significant long-term contributing factor to the brain tissue response to the persistence of an implanted silicon microelectrode array in cortical brain tissue.

The region around chronic microelectrodes most depleted of neurons correlated strongly with the presence of intense ED1 immunoreactivity. This observation can be explained by several hypotheses: (1) macrophage activation leads to neuronal loss, (2) high macrophage activation results from neuronal damage due to another mechanism, and (3) neurons are displaced from the electrode surface by the inflammatory reaction. The latter two observations are

not consistent with our observations. The persistence of the activated macrophage layer suggests an inability to resolve the inflammatory response. The death of a finite number of cells in the vicinity of the microelectrode would not be expected to produce an extended inflammatory response, as the cells would likely be removed and the wound healing response would resolve on a time scale similar to that observed with the stab wound controls. Rather, the persistence of inflammatory response is more consistent with a response of a persistent stimulus. If neurons were pushed from the microelectrode surface by the astroglial response, one would expect to find an increased density of neurons outside the excluding inflammatory zone. No such pattern was observed. Instead, neurofilament loss significantly expanded beyond the inflammatory zone and into the adjacent neuropil by 4 weeks p.i.

The effective recording range of this and similar types of microelectrodes, defined as the maximum distance from which single units can be resolved, is reported under ideal

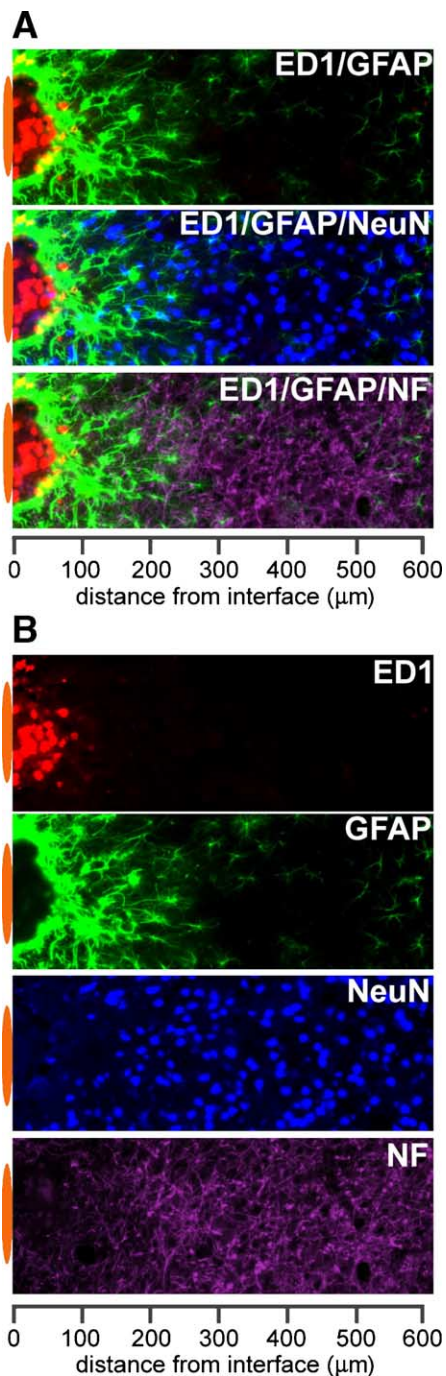


Fig. 6. Stratification of cellular immunoreactivity using cell-type-specific markers at the microelectrode–brain tissue interface. Representative images collected from two adjacent sections of an animal with a 4-week microelectrode implant illustrate the general appearance of the foreign body response characterized by minimally overlapping inflammatory (ED1) and astrocytic (GFAP) phenotypes adjacent to the implant interface. The area of inflammation and intense astrocyte reactivity contains a reduced number of NeuN<sup>+</sup> neuronal bodies and a loss of neurofilament (NF) density. The position of the microelectrode is illustrated by the orange oval (drawn to scale) at the left of each image. Images were captured in grayscale and pseudocolored for illustration.

conditions to be approximately a 130- $\mu\text{m}$  from the recording electrode surface to a nearby neuronal cell body (Drake et al., 1988; Henze et al., 2000). However, it has been reported experimentally that the best cluster separation of single units in the hippocampus was obtained from neurons residing within a much smaller distance from the microelectrode-recording surface. Reductions in resolving capability of single units were encountered when recording beyond this distance (Henze et al., 2000). We observed a 40% decline in the number of neuronal bodies within a 100- $\mu\text{m}$  radius of the microelectrode in the cerebral cortex and a significant loss of neurofilament expression as far away as 230  $\mu\text{m}$ . Such reductions would be expected to significantly reduce the probability of establishing and maintaining stable long-term recording from neurons.

While the current study establishes a strong correlation between microelectrode-mediated inflammation and the loss of neurons, more studies will be required to understand the precise biological mechanisms involved. Although the absence of positive neuronal immunoreactivity using two independent markers strongly suggests neuronal death, it is unclear if this occurs as a result of necrosis or an apoptosis, or a combination. It will also be important to examine the response over more time points. By 2 weeks, we observed that a relatively large amount of neuronal loss was already evident, and thus it will be important to examine the response earlier to identify the critical period of relatively extensive neuronal loss and whether pharmacological agents that reduce microglial activation can reduce this.

Accumulating evidence from postmortem analysis of patients that have received deep brain stimulating electrode implants for the treatment of movement disorders suggests that chronic neuroinflammation is a part of the foreign body response to such implants as well. Studies with indwelling times that vary from less than 2 years to over 7 years provide a consistent picture of a brain tissue response that is characterized by extensive gliosis surrounding the entire length of the electrode tract, the presence of macrophages, tissue vacuolation, and cell loss up to 1 mm from the implant surface (Caparros-Lefebvre et al., 1994; Haberler et al., 2000; Henderson et al., 2002; Kuroda et al., 1991). From a stimulation and neurosurgical perspective, the persistent inflammation and cell loss observed at the implant–brain tissue interface may be an appropriate risk given the therapeutic benefit of such devices; however, from an action potential single unit recording perspective, neuronal loss at distances greater than 100  $\mu\text{m}$  is insurmountable.

In summary, our findings suggest a novel mechanism underlying the loss of recording capability frequently observed with chronic applications of planar silicon microelectrode arrays. It follows that manipulation of the inflammatory response would be expected to improve the brain tissue response and long-term performance of chronically implanted silicon microelectrode arrays, particularly with designs where the recording sites are located along the microelectrode shaft and adjacent to the reactive zone.

## Acknowledgments

The authors gratefully acknowledge the contributions of Ms. Mindy Naegle, Lindsey Alder, and Dr. Elena Budko for their technical assistance. Multichannel planar silicon microelectrode arrays were provided by the University of Michigan Center for Neural Communication Technology sponsored by NIH NIBIB grant P41-RR09754. Funding support was provided by the National Institutes of Health (NINDS N01-NS-1-2338).

## References

- Aebischer, P., Winn, S.R., Galletti, P.M., 1988. Transplantation of neural tissue in polymer capsules. *Brain Res.* 448, 364–368.
- Agnew, W.F., Yuen, T.G., McCreery, D.B., Bullara, L.A., 1986. Histopathologic evaluation of prolonged intracortical electrical stimulation. *Exp. Neurol.* 92, 162–185.
- Banati, R.B., Gehrmann, J., Schubert, P., Kreutzberg, G.W., 1993. Cytotoxicity of microglia. *Glia* 7, 111–118.
- Behling, C.A., Spector, M., 1986. Quantitative characterization of cells at the interface of long-term implants of selected polymers. *J. Biomed. Mater. Res.* 20, 653–666.
- Bottenstein, J.E., Sato, G.H., 1979. Growth of a rat neuroblastoma cell line in serum-free supplemented medium. *Proc. Natl. Acad. Sci. U. S. A.* 76, 514–517.
- Branner, A., Stein, R.B., Normann, R.A., 2001. Selective stimulation of cat sciatic nerve using an array of varying-length microelectrodes. *J. Neurophysiol.* 85, 1585–1594.
- Campioni, E.G., Nobrega, J.N., Sefton, M.V., 1998. HEMA/MMMA microcapsule implants in hemiparkinsonian rat brain: biocompatibility assessment using [3H]PK11195 as a marker for gliosis. *Biomaterials* 19, 829–837.
- Caparros-Lefebvre, D., Ruchoux, M.M., Blond, S., Petit, H., Percheron, G., 1994. Long-term thalamic stimulation in Parkinson's disease: post-mortem anatomoclinical study. *Neurology* 44, 1856–1860.
- Carter, R., Houk, J., 1993. Multiple single-unit recordings from the CNS using thin-film electrode arrays. *IEEE Trans. Rehab. Eng.* 1, 175–184.
- Cavanagh, J.B., 1970. The proliferation of astrocytes around a needle wound in the rat brain. *J. Anat.* 106, 471–487.
- Colton, C.A., Chernyshev, O.N., Gilbert, D.L., Vitek, M.P., 2000. Microglial contribution to oxidative stress in Alzheimer's disease. *Ann. N. Y. Acad. Sci.* 899, 292–307.
- Csicsvari, J., Henze, D.A., Jamieson, B., Harris, K.D., Sirota, A., Bartho, P., Wise, K.D., Buzsaki, G., 2003. Massively parallel recording of unit and local field potentials with silicon-based electrodes. *J. Neurophysiol.* 90, 1314–1323.
- Drake, K.L., Wise, K.D., Farraye, J., Anderson, D.J., BeMent, S.L., 1988. Performance of planar multisite microprobes in recording extracellular single-unit intracortical activity. *IEEE Trans. Biomed. Eng.* 35, 719–732.
- Dymond, A.M., Kaechele, L.E., Jurist, J.M., Crandall, P.H., 1970. Brain tissue reaction to some chronically implanted metals. *J. Neurosurg.* 33, 574–580.
- Edell, D.J., Toi, V.V., McNeil, V.M., Clark, L.D., 1992. Factors influencing the biocompatibility of insertable silicon microshafts in cerebral cortex. *IEEE Trans. Biomed. Eng.* 39, 635–643.
- Gasque, P., Dean, Y.D., McGreal, E.P., VanBeek, J., Morgan, B.P., 2000. Complement components of the innate immune system in health and disease in the CNS. *Immunopharmacology* 49, 171–186.
- Goldring, S.R., Clark, C.R., Wright, T.M., 1993. The problem in total joint arthroplasty: aseptic loosening. *J. Bone Joint Surg. Am.* 75, 799–801.
- Haberler, C., Alesch, F., Mazal, P.R., Pilz, P., Jellinger, K., Pinter, M.M., Hainfellner, J.A., Budka, H., 2000. No tissue damage by chronic deep brain stimulation in Parkinson's disease. *Ann. Neurol.* 48, 372–376.
- Hanisch, U.K., 2002. Microglia as a source and target of cytokines. *Glia* 40, 140–155.
- Henderson, J.M., Pell, M., O'Sullivan, D.J., McCusker, E.A., Fung, V.S., Hedges, P., Halliday, G.M., 2002. Postmortem analysis of bilateral subthalamic electrode implants in Parkinson's disease. *Mov. Disord.* 17, 133–137.
- Henze, D.A., Borhegyi, Z., Csicsvari, J., Mamiya, A., Harris, K.D., Buzsaki, G., 2000. Intracellular features predicted by extracellular recordings in the hippocampus in vivo. *J. Neurophysiol.* 84, 390–400.
- Janatova, J., 2000. Activation and control of complement, inflammation, and infection associated with the use of biomedical polymers. *ASAIO J.* 46, S53–S62.
- Kim, Y., Hitchcock, R., Bridge, M., Tresco, P., 2004. Chronic response of adult rat brain tissue to implants anchored to the skull. *Biomaterials* 25 (12), 2229–2237.
- Kipke, D.R., Vetter, R.J., Williams, J.C., Hetke, J.F., 2003. Silicon-substrate intracortical microelectrode arrays for long-term recording of neuronal spike activity in cerebral cortex. *IEEE Trans. Neural Syst. Rehabil. Eng.* 11, 151–155.
- Kuroda, R., Nakatani, J., Yamada, Y., Yorimae, A., Kitano, M., 1991. Location of a DBS-electrode in lateral thalamus for deafferentation pain. An autopsy case report. *Acta Neurochir. Suppl. (Wien)* 52, 140–142.
- Liu, X., McCreery, D.B., Carter, R.R., Bullara, L.A., Yuen, T.G., Agnew, W.F., 1999. Stability of the interface between neural tissue and chronically implanted intracortical microelectrodes. *IEEE Trans. Rehabil. Eng.* 7, 315–326.
- Liu, B., Gao, H.M., Wang, J.Y., Jeohn, G.H., Cooper, C.L., Hong, J.S., 2002. Role of nitric oxide in inflammation-mediated neurodegeneration. *Ann. N. Y. Acad. Sci.* 962, 318–331.
- Luber-Narod, J., Rogers, J., 1988. Immune system associated antigens expressed by cells of the human central nervous system. *Neurosci. Lett.* 94, 17–22.
- Mathewson, A.J., Berry, M., 1985. Observations on the astrocyte response to a cerebral stab wound in adult rats. *Brain Res.* 327, 61–69.
- McCreery, D.B., Yuen, T.G., Agnew, W.F., Bullara, L.A., 1997. A characterization of the effects on neuronal excitability due to prolonged microstimulation with chronically implanted microelectrodes. *IEEE Trans. Biomed. Eng.* 44, 931–939.
- McGeer, P.L., Akiyama, H., Itagaki, S., McGeer, E.G., 1989. Activation of the classical complement pathway in brain tissue of Alzheimer patients. *Neurosci. Lett.* 107, 341–346.
- Nicolelis, M.A., Ribeiro, S., 2002. Multielectrode recordings: the next steps. *Curr. Opin. Neurobiol.* 12, 602–606.
- Picha, G.J., Goldstein, J.A., Stohr, E., 1990. Natural-Y Meme polyurethane versus smooth silicone: analysis of the soft-tissue interaction from 3 days to 1 year in the rat animal model. *Plast. Reconstr. Surg.* 85, 903–916.
- Powell, E.M., Sobarzo, M.R., Saltzman, W.M., 1990. Controlled release of nerve growth factor from a polymeric implant. *Brain Res.* 515, 309–311.
- Roitbak, T., Sykova, E., 1999. Diffusion barriers evoked in the rat cortex by reactive astrogliosis. *Glia* 28, 40–48.
- Rothstein, J.D., Jin, L., Dykes-Hoberg, M., Kuncl, R.W., 1993. Chronic inhibition of glutamate uptake produces a model of slow neurotoxicity. *Proc. Natl. Acad. Sci. U. S. A.* 90, 6591–6595.
- Schmidt, E.M., Bak, M.J., McIntosh, J.S., 1976. Long-term chronic recording from cortical neurons. *Exp. Neurol.* 52, 496–506.
- Schmidt, S., Horch, K., Normann, R., 1993. Biocompatibility of silicon-based electrode arrays implanted in feline cortical tissue. *J. Biomed. Mater. Res.* 27, 1393–1399.

- Schultz, R.L., Willey, T.J., 1976. The ultrastructure of the sheath around chronically implanted electrodes in brain. *J. Neurocytol.* 5, 621–642.
- Singhroo, S.K., Neal, J.W., Rushmere, N.K., Morgan, B.P., Gasque, P., 2000. Spontaneous classical pathway activation and deficiency of membrane regulators render human neurons susceptible to complement lysis. *Am. J. Pathol.* 157, 905–918.
- Stensaas, S.S., Stensaas, L.J., 1976. The reaction of the cerebral cortex to chronically implanted plastic needles. *Acta Neuropathol. (Berl.)* 35, 187–203.
- Stensaas, S.S., Stensaas, L.J., 1978. Histopathological evaluation of materials implanted in the cerebral cortex. *Acta Neuropathol. (Berl.)* 41, 145–155.
- Sutherland, K., Mahoney II, J.R., Coury, A.J., Eaton, J.W., 1993. Degradation of biomaterials by phagocyte-derived oxidants. *J. Clin. Invest.* 92, 2360–2367.
- Szarowski, D.H., Andersen, M.D., Retterer, S., Spence, A.J., Isaacson, M., Craighead, H.G., Turner, J.N., Shain, W., 2003. Brain responses to micro-machined silicon devices. *Brain Res.* 983, 23–35.
- Tang, L., Ugarova, T.P., Plow, E.F., Eaton, J.W., 1996. Molecular determinants of acute inflammatory responses to biomaterials. *J. Clin. Invest.* 97, 1329–1334.
- Turner, J.N., Shain, W., Szarowski, D.H., Andersen, M., Martins, S., Isaacson, M., Craighead, H., 1999. Cerebral astrocyte response to micromachined silicon implants. *Exp. Neurol.* 156, 33–49.
- Vitkovic, L., Bockaert, J., Jacque, C., 2000. “Inflammatory” cytokines: neuromodulators in normal brain? *J. Neurochem.* 74, 457–471.
- Winn, S.R., Aebischer, P., Galletti, P.M., 1989. Brain tissue reaction to permselective polymer capsules. *J. Biomed. Mater. Res.* 23, 31–44.
- Yuen, T.G., Agnew, W.F., 1995. Histological evaluation of polyesterimide-insulated gold wires in brain. *Biomaterials* 16, 951–956.